Ne-like Ca XI—Mn XVI $2p^5 3l$-$2p^5 4l$ transition arrays and energy levels

C. Jupén and U. Litzén
Physics Department, University of Lund, S-22362 Lund, Sweden

V. Kaufman and J. Sugar
National Bureau of Standards, Gaithersburg, Maryland 20899
(Received 7 August 1986)

Spectra from laser-produced plasmas of Ca, Sc, Ti, V, Cr, and Mn have been recorded in the grazing-incidence region, and the transition arrays $3s$-$4p$, $3p$-$4s$, $3p$-$4d$, and $3d$-$4f$ of the neonlike ions have been identified. The measured wavelengths together with the previously observed 3-3 transitions have been used for deriving energy levels of the $2s^2 2p^5 3l$ and $2s^2 2p^5 4l$ configurations. The term structure has been analyzed by means of *ab initio* and parametric calculations and isoelectronic relations. Coupling conditions have been studied and eigenvectors have been derived. Significant perturbations caused by the $2s2p^6 nl$ configurations have been investigated.

I. INTRODUCTION

The $2p^5 3s$, $3p$, and $3d$ configurations of highly charged ions in the neonlike isoelectronic sequence have been the object of several investigations during recent years. The interest in these ions has to a great extent been stimulated by the possibility of obtaining laser action in certain $3s$-$3p$ lines in the extreme ultraviolet region[1,2] and by the identifications of $3s$-$3p$ and $3p$-$3d$ lines of Fe XVII in solar-flare spectra.[3,4] Thus $3s$-$3p$ and $3p$-$3d$ transitions in the region 200—700 Å have been identified in Ca XI—Mn XVI in spectra emitted from laser-produced plasmas,[5–7] and in Ti XIII, Cr XV, and Fe XVII in beam-foil experiments.[8–10] The level structure of these configurations was analyzed by means of Slater-Condon theory in Ca XI, Ti XIII, and Fe XVII,[5,6] and the derived scaling factors for the Slater parameters could be used for predictions of the level structure and transition wavelengths. Several *ab initio* studies of these configurations have also been published.[11–14]

In the present work transitions between the $2p^5 3l$ and $2p^5 4l$ configurations in neonlike Ca XI—Mn XVI have been identified in spectra from laser-produced plasmas. Identifications of the strongest lines of 3-4 transition arrays have previously been reported by Fawcett *et al.*,[15] but that investigation appears to have been hampered by a low spectral resolution and by the lack of information on the $2p^5 3l$ structure. The strongest $3p$-$4d$ lines were also observed by Kastner *et al.*[16] All observed 3-3 and 3-4 transitions have now been used for deriving energy levels of the $2p^5 3l$ and $2p^5 4l$ configurations. As a result all the levels of $3s$, $3p$, $3d$, $4d$, and $4f$ in Ca XI—Mn XVI are now

TABLE I. Measured wavelengths of $2p^5 3p$-$2p^5 4s$ transitions in the Ne I sequence.

	Ca XI		Sc XII		Ti XIII		Cr XV		Mn XVI	
	I	λ (Å)	I	λ (Å)	I	λ (Å)	I	λ (Å)	I	λ (Å)
$3p(\frac{3}{2})[\frac{1}{2}]_1$-$4s(\frac{3}{2},\frac{1}{2})_1$							1	70.428		
$3p(\frac{3}{2})[\frac{1}{2}]_1$-$4s(\frac{3}{2},\frac{1}{2})_2$							4	70.728		
$3p(\frac{3}{2})[\frac{5}{2}]_2$-$4s(\frac{3}{2},\frac{1}{2})_1$							10	71.845		
$3p(\frac{1}{2})[\frac{3}{2}]_1$-$4s(\frac{1}{2},\frac{1}{2})_0$							1	71.975		
$3p(\frac{3}{2})[\frac{5}{2}]_2$-$4s(\frac{3}{2},\frac{1}{2})_2$	1	129.140	1	109.876			5	72.157		
$3p(\frac{3}{2})[\frac{5}{2}]_3$-$4s(\frac{3}{2},\frac{1}{2})_2$	3	129.191	1	110.030	2	94.788	20	72.511	5	64.224
$3p(\frac{3}{2})[\frac{3}{2}]_1$-$4s(\frac{3}{2},\frac{1}{2})_1$							1	72.692		
$3p(\frac{1}{2})[\frac{1}{2}]_1$-$4s(\frac{1}{2},\frac{1}{2})_1$							5	72.849		
$3p(\frac{1}{2})[\frac{3}{2}]_2$-$4s(\frac{1}{2},\frac{1}{2})_1$							2	72.941		
$3p(\frac{1}{2})[\frac{1}{2}]_1$-$4s(\frac{1}{2},\frac{1}{2})_0$							1	72.971		
$3p(\frac{3}{2})[\frac{3}{2}]_2$-$4s(\frac{3}{2},\frac{1}{2})_1$							3	73.286		
$3p(\frac{3}{2})[\frac{3}{2}]_2$-$4s(\frac{3}{2},\frac{1}{2})_2$			1	112.076	1	96.429	5	73.627	2	65.153

TABLE II. Measured wavelengths of $2p^53s$-$2p^54p$ transitions in the Ne I sequence.

	Ca XI		Sc XII		Ti XIII		V XIV		Cr XV		Mn XVI	
	I	λ (Å)	I	λ (Å)	I	λ (Å)	I	λ (Å)	I	λ (Å)	I	λ (Å)
$3s(\frac{3}{2},\frac{1}{2})_2\text{-}4p(\frac{3}{2})[\frac{3}{2}]_2$									2	57.775		
$3s(\frac{3}{2},\frac{1}{2})_2\text{-}4p(\frac{3}{2})[\frac{5}{2}]_3$	10	98.422	4	85.163	2	74.108	3	65.330	10	58.008	3	51.847
$3s(\frac{3}{2},\frac{1}{2})_2\text{-}4p(\frac{3}{2})[\frac{5}{2}]_2$									3	58.107		
$3s(\frac{3}{2},\frac{1}{2})_1\text{-}4p(\frac{3}{2})[\frac{3}{2}]_1$ $3s(\frac{3}{2},\frac{1}{2})_2\text{-}4p(\frac{3}{2})[\frac{1}{2}]_1$									10	58.350	2	52.147
$3s(\frac{1}{2},\frac{1}{2})_1\text{-}4p(\frac{1}{2})[\frac{3}{2}]_2$	10	98.908	2	85.456			1	65.571	2	58.194	2	51.999
$3s(\frac{3}{2},\frac{1}{2})_1\text{-}4p(\frac{3}{2})[\frac{5}{2}]_2$									3	58.555	1	52.344
$3s(\frac{1}{2},\frac{1}{2})_1\text{-}4p(\frac{1}{2})[\frac{3}{2}]_1$									1	58.469		

known, or predictable with high accuracy. Concerning $4s$ and $4p$, a number of levels are still missing in certain ions. This is due to the low intensity of the $3s$-$4p$ and $3p$-$4s$ transitions, and the irregularities in the isoelectronic trends of wave numbers and energy levels caused by perturbations from the core-excited $2s2p^63l$ configurations.

II. EXPERIMENT

The spectra of highly ionized calcium, scandium, titanium, vanadium, chromium, and manganese were emitted from plasmas produced by focusing a Nd-glass pulsed laser beam with a power of 1 GW and pulse width of 15 ns onto solid metal targets. The spectra were recorded on Kodak 101-05 plates with the 10.7-m grazing-incidence spectrograph at the National Bureau of Standards, Washington, D.C. A slit width of 50 μm was used, and about 20 laser pulses were needed to produce satisfactory exposures. For plate calibration we used laser-generated spectra of Y XI–XIV and Mo XIV–XVII with the wavelengths reported in Refs. 17–21 with an uncertainty of ± 0.005 Å. We estimate our wavelength uncertainty to be at most ± 0.005–0.01 Å.

III. SPECTRAL LINES

All the lines included in the present work are given in Tables I–IV, containing the transition arrays $3s$-$4p$, $3p$-$4s$, $3p$-$4d$, and $3d$-$4f$. The strongest spectrum and consequently the most complete transition arrays were obtained in chromium, where furthermore the structure of the neonlike $n=4$ configurations is essentially unaffected by the perturbations to be discussed below. For these reasons the identification work was started in chromium. We

TABLE III. Measured wavelengths of $2p^53p$-$2p^54d$ transitions in the Ne I sequence.

	Ca XI		Sc XII		Ti XIII		V XIV		Cr XV		Mn XVI	
	I	λ (Å)	I	λ (Å)	I	λ (Å)	I	λ (Å)	I	λ (Å)	I	λ (Å)
$3p(\frac{3}{2})[\frac{1}{2}]_1\text{-}4d(\frac{3}{2})[\frac{3}{2}]_2$	1	105.348	2	90.727	1	79.004			3	61.460	2	54.832
$3p(\frac{3}{2})[\frac{1}{2}]_1\text{-}4d(\frac{3}{2})[\frac{1}{2}]_1$			3	91.007	1	79.235	1	69.609	5	61.639	1	54.988
$3p(\frac{3}{2})[\frac{1}{2}]_1\text{-}4d(\frac{3}{2})[\frac{1}{2}]_0$							2	69.726	1	61.746	1	55.09
$3p(\frac{3}{2})[\frac{3}{2}]_1\text{-}4d(\frac{3}{2})[\frac{3}{2}]_1$									2	62.233	1	55.472
$3p(\frac{3}{2})[\frac{5}{2}]_2\text{-}4d(\frac{3}{2})[\frac{5}{2}]_2$	1	107.668					1	70.487	4	62.318	1	55.517
$3p(\frac{1}{2})[\frac{3}{2}]_1\text{-}4d(\frac{1}{2})[\frac{5}{2}]_2$	2	107.928	4	92.687	3	80.502	2	70.573	10	62.378	5	55.560
$3p(\frac{3}{2})[\frac{5}{2}]_2\text{-}4d(\frac{3}{2})[\frac{7}{2}]_3$	5	108.006	6	92.787	5	80.610	5	70.677	25	62.485	10	55.659
$3p(\frac{3}{2})[\frac{5}{2}]_3\text{-}4d(\frac{3}{2})[\frac{5}{2}]_3$											2	55.728
$3p(\frac{3}{2})[\frac{5}{2}]_3\text{-}4d(\frac{3}{2})[\frac{7}{2}]_3$			1	92.901					3	62.754	1	55.962
$3p(\frac{3}{2})[\frac{5}{2}]_3\text{-}4d(\frac{3}{2})[\frac{7}{2}]_4$	10	108.249	20	93.075	10	80.927	10	71.022	50	62.842	15	56.032
$3p(\frac{3}{2})[\frac{3}{2}]_1\text{-}4d(\frac{3}{2})[\frac{5}{2}]_2$	2	108.669	5	93.390	3	81.153	4	71.187	10	62.958	3	56.110
$3p(\frac{1}{2})[\frac{3}{2}]_2\text{-}4d(\frac{1}{2})[\frac{5}{2}]_3$	7	108.811	10	93.506	5	81.258	4	71.290	40	63.016	5	56.207
$3p(\frac{1}{2})[\frac{1}{2}]_1\text{-}4d(\frac{1}{2})[\frac{3}{2}]_2$	2	108.984	3	93.612	2	81.322	2	72.317				
$3p(\frac{3}{2})[\frac{3}{2}]_2\text{-}4d(\frac{3}{2})[\frac{5}{2}]_3$	4	109.317	10	93.924	10	81.611	5	71.589			5	56.432
$3p(\frac{3}{2})[\frac{3}{2}]_2\text{-}4d(\frac{3}{2})[\frac{3}{2}]_2$	1	109.992	1	94.470					3	63.637	2	56.700

TABLE IV. Measured wavelengths of $2p^5 3d$-$2p^5 4f$ transitions in the Ne I sequence.

	Ca XI		Sc XII		Ti XIII		V XIV		Cr XV		Mn XVI	
	I	λ (Å)	I	λ (Å)	I	λ (Å)	I	λ (Å)	I	λ (Å)	I	λ (Å)
$3d(\frac{3}{2})[\frac{1}{2}]_0$-$4f(\frac{3}{2})[\frac{3}{2}]_1$			4	113.008	2	97.358	3	84.420	10	73.884	6	65.216
$3d(\frac{3}{2})[\frac{1}{2}]_1$-$4f(\frac{3}{2})[\frac{3}{2}]_2$	4	132.577	10	113.926	5	97.758	5	84.757	20	74.173	8	65.470
$3d(\frac{3}{2})[\frac{1}{2}]_1$-$4f(\frac{3}{2})[\frac{3}{2}]_1$									9	74.029	4	65.508
$3d(\frac{3}{2})[\frac{3}{2}]_2$-$4f(\frac{3}{2})[\frac{5}{2}]_3$	5	135.217	8	114.903	10	98.490	20	85.360	60	74.695 }	30	65.927
$3d(\frac{3}{2})[\frac{7}{2}]_4$-$4f(\frac{3}{2})[\frac{7}{2}]_4$	2	136.830	9	115.433			15	85.482	8	74.738 }		
$3d(\frac{3}{2})[\frac{3}{2}]_2$-$4f(\frac{3}{2})[\frac{3}{2}]_2$									10	74.813	4	66.036
$3d(\frac{3}{2})[\frac{7}{2}]_4$-$4f(\frac{3}{2})[\frac{9}{2}]_5$	30	137.319	20	115.837	30	99.074	60	85.758	100	74.975	50	66.129
$3d(\frac{3}{2})[\frac{7}{2}]_3$-$4f(\frac{3}{2})[\frac{7}{2}]_4$									7	75.054		
$3d(\frac{3}{2})[\frac{7}{2}]_3$-$4f(\frac{3}{2})[\frac{7}{2}]_3$			4	116.069			10	85.899	3	75.084	3	66.209
$3d(\frac{3}{2})[\frac{7}{2}]_3$-$4f(\frac{3}{2})[\frac{9}{2}]_4$	40	138.070	20	116.445 }	50	99.572	80*bl*	86.148	90	75.297	40	66.393
$3d(\frac{1}{2})[\frac{5}{2}]_2$-$4f(\frac{1}{2})[\frac{7}{2}]_3$	10	138.302	12	116.535 }			15	86.125	50	75.241	20	66.320
$3d(\frac{1}{2})[\frac{3}{2}]_2$-$4f(\frac{1}{2})[\frac{5}{2}]_3$			15	116.760	15	99.834	20	86.356	70	75.446	30	66.503
$3d(\frac{1}{2})[\frac{5}{2}]_3$-$4f(\frac{1}{2})[\frac{5}{2}]_3$									1	75.605		
$3d(\frac{3}{2})[\frac{5}{2}]_2$-$4f(\frac{3}{2})[\frac{5}{2}]_2$			1	117.043								
$3d(\frac{1}{2})[\frac{5}{2}]_3$-$4f(\frac{1}{2})[\frac{7}{2}]_4$	50	139.052	20	117.172	25	100.133	40	86.609	90	75.670	60	66.706
$3d(\frac{3}{2})[\frac{5}{2}]_2$-$4f(\frac{3}{2})[\frac{7}{2}]_3$	20	139.025	5	117.209	15	100.200	30	86.684	90	75.743	50	66.773
$3d(\frac{3}{2})[\frac{5}{2}]_2$-$4f(\frac{3}{2})[\frac{3}{2}]_2$									1	75.886		
$3d(\frac{3}{2})[\frac{5}{2}]_3$-$4f(\frac{3}{2})[\frac{5}{2}]_3$	1	138.800	3	117.735					25	76.162	3	67.149
$3d(\frac{3}{2})[\frac{5}{2}]_3$-$4f(\frac{3}{2})[\frac{7}{2}]_4$	20	139.900	15	117.901	20	100.753	60	87.141	100	76.125	60	67.099
$3d(\frac{3}{2})[\frac{5}{2}]_3$-$4f(\frac{3}{2})[\frac{9}{2}]_4$									6	76.371	2	67.314
$3d(\frac{3}{2})[\frac{3}{2}]_1$-$4f(\frac{3}{2})[\frac{5}{2}]_2$			2	120.226	7	102.964	5	89.103	10	77.874	7	68.662
$3d(\frac{1}{2})[\frac{3}{2}]_1$-$4f(\frac{1}{2})[\frac{5}{2}]_2$					2	104.593	5	90.227	10	78.625	5	69.124

made use of the regular isoelectronic trends of the wave numbers shown in Figs. 1 and 2 and the derived scaling of the Slater parameters.

The level designations in Tables I—IV are given in *jj* and *jl* notation, and will be further discussed below.

IV. ENERGY LEVELS

The neonlike ions are characterized by the large energy gap between the ground state $2p^6\,{}^1S_0$ (see Fig. 3) and the first excited configuration $2p^5 3s$. Thus the absolute energy scale of the term system is established through lines in the soft-x-ray region. In the present work the excited levels were connected to the ground state by means of the transitions from $3s(\frac{1}{2},\frac{1}{2})_1$ and $3s(\frac{3}{2},\frac{1}{2})_1$ measured by Edlén and Tyrén[22] and Tyrén,[23] and quoted in the NBS compilations of iron-group energy levels.[24]

The 3-4 transitions from the present work and 3-3 transitions from previous investigations have been used for deriving the $2p^5 3l$ and $2p^5 4l$ levels of Ca XI—Mn XVI. With a few exceptions, the 3-3 lines were taken from the recordings of laser-produced plasmas in Refs. 5—7. The lines of the neonlike ions are obviously much more prominent in the beam-foil recordings in Refs. 8—10 than in the laser-produced plasmas of Refs. 5—7, but the wavelength accuracy is higher in the latter case. For this reason, only wavelengths of lines that were not observed in the plasma investigations have been taken from the beam-foil work. In particular it should be noted that the beam-foil wavelength for $3s(\frac{3}{2},\frac{1}{2})_2$-$3p(\frac{3}{2})[\frac{1}{2}]_1$, 551.60 Å,[8] has replaced the erroneous wavelength for this line in Ref. 5. Furthermore, the analysis of the $n=3$ configurations has shown that two lines reported in Ref. 7 have to be discarded, viz., 342.202 Å in V XIV and 377.414 Å in Mn XVI.

The derived $2p^5 3l$ and $2p^5 4l$ energy levels are given in Tables V, VI, and VII. Predicted values, obtained from parametric calculations to be discussed below, are inserted in parentheses in cases were no level values could be derived from the observations. In $4s$ and $4p$, the small number of observed levels make the parametric calculations rather uncertain, and therefore predicted values are not given.

It has not been possible to find $3s$-$3p$ or $3s$-$4p$ lines that can be used for establishing the position of $3s(\frac{1}{2},\frac{1}{2})_0$ relative to the rest of the $3s$ levels in V XIV and Mn XVI. This level is, however, crucial for the derivation of certain level values of the higher configurations, and its position has therefore been determined through isoelectronic interpolation of the $3s(\frac{1}{2},\frac{1}{2})_1$-$(\frac{1}{2},\frac{1}{2})_0$ interval. The regular trend of this interval and the $3s(\frac{3}{2},\frac{1}{2})_1$-$(\frac{3}{2},\frac{1}{2})_2$ interval is shown in Fig. 4, where the Fe XVII data were taken from Ref. 4. The values for the $J=0$ level of $3s$ in V XIV and Mn XVI obtained from a least-squares fit of a straight line to the $3s(\frac{1}{2},\frac{1}{2})_1$-$(\frac{1}{2},\frac{1}{2})_0$ interval for Ca XI—Fe XVII are given in Table V. They are believed to be more accurate than the values from parametric calculations.

The high probabilities for transitions from the odd $J=1$ levels to the ground state lead to unfavorable branching ratios for transitions to other excited levels, and with the exception of $3s$, many of the odd $J=1$ levels are therefore badly or not at all connected to the rest of the excited system. In such cases the level values derived from x-ray transitions to the ground state as quoted in Ref. 24 are given in Tables V, VI, and VII. For $3d$ and $4d$ the values from the parametric calculations are also shown for these levels. In $3d$ the agreement is in most cases good, while some serious deviations are found in $4d$. Relative to the rest of the excited levels, the calculated level values are believed to be better than the x-ray values.

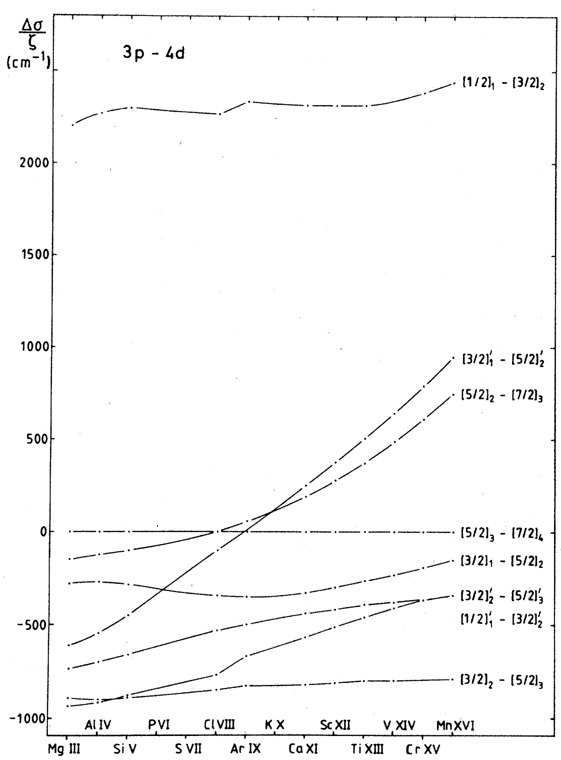

FIG. 1. Wave-number differences divided by the core charge ζ plotted versus ζ for the strongest $3p$-$4d$ lines in Mg III—Mn XVI. The abbreviated notation $[K]$ is used for $(\frac{3}{2})[K]$ and $[K]'$ for $(\frac{1}{2})[K]$. $\Delta\sigma$ is the distance from the $3p[\frac{5}{2}]_3$-$4d[\frac{7}{2}]_4$ line. The deviations from the smooth behavior of some of the curves at Cl VIII and Ar IX are due to interaction between $2s^22p^54d$ and $2s2p^63p$; cf. the text and Fig. 6.

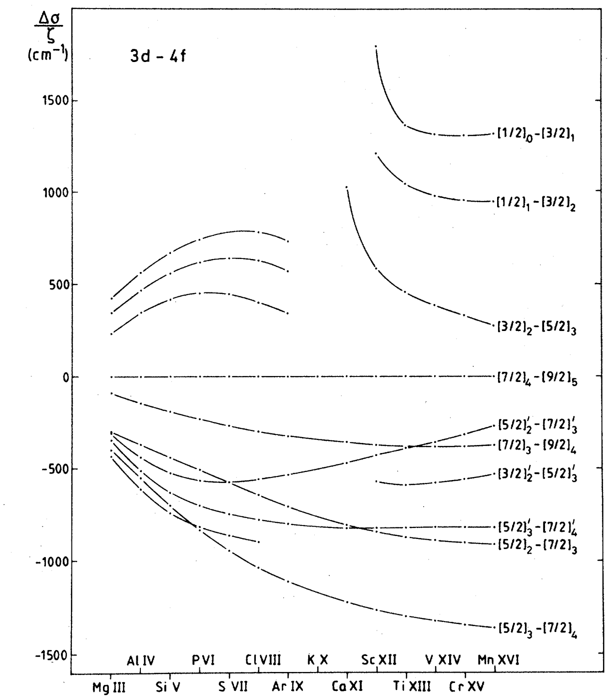

FIG. 2. Wave-number differences divided by the core charge for the strongest $3d$-$4f$ lines in Mg III—Mn XVI. The abbreviated designations are explained in the text of Fig. 1. The strong irregularities in some of the curves are due to perturbations of certain $4f$ levels, evident in Fig. 7.

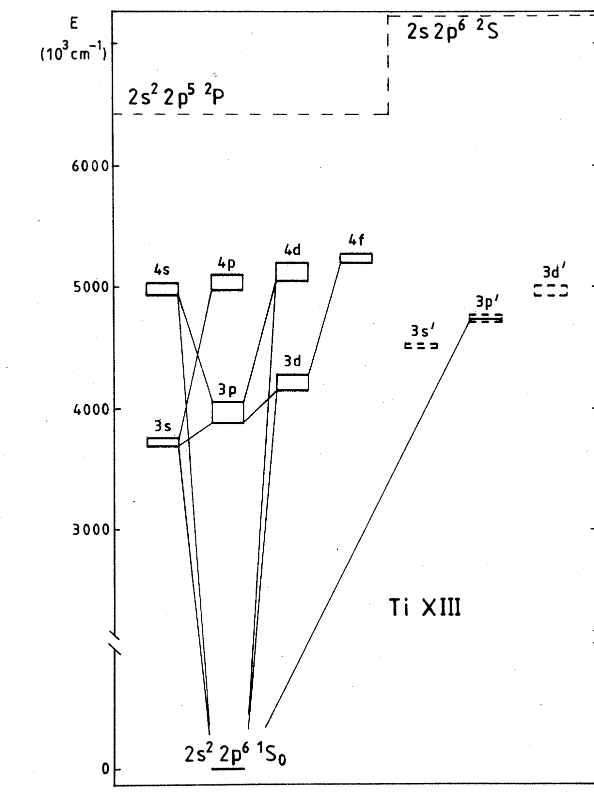

FIG. 3. Survey term diagram of Ti XIII showing the $n=3$ and $n=4$ configurations.

TABLE V. Energy levels (cm^{-1}) of the $2p^5 3l$ configurations.

Designation	J	Ca XI	Sc XII	Ti XIII	V XIV	Cr XV	Mn XVI	Eigenvector components (%)[a] Ca XI		Mn XVI		LS designation[b]
$3s(\frac{3}{2},\frac{1}{2})$	2	2 802 080	3 235 171	3 698 153	4 190 606	4 714 294	5 266 964	$100(\frac{3}{2},\frac{1}{2})$		$100(\frac{3}{2},\frac{1}{2})$		^3P
	1	2 810 900[c]	3 245 100[c]	3 709 200[c]	4 202 700[c]	4 727 500[c]	5 281 200[c]	$92(\frac{3}{2},\frac{1}{2})$		$98(\frac{3}{2},\frac{1}{2})$		^3P
$3s(\frac{1}{2},\frac{1}{2})$	1	2 839 900[c]	3 280 800[c]	3 753 600[c]	4 257 100[c]	4 793 200[c]	5 360 800[c]	$92(\frac{1}{2},\frac{1}{2})$		$98(\frac{1}{2},\frac{1}{2})$		^1P
	0	2 832 095	3 272 730	3 745 238	4 248 410[d]	4 784 174	5 351 520[d]	$100(\frac{1}{2},\frac{1}{2})$		$100(\frac{1}{2},\frac{1}{2})$		^3P
$3p(\frac{3}{2})[\frac{5}{2}]$	3	2 978 449	3 428 533	3 908 849	4 419 174	4 961 187	5 532 778	$100(\frac{3}{2})[\frac{5}{2}]$		$100(\frac{3}{2})[\frac{5}{2}]$		^3D
	2	2 978 212	3 427 225	3 906 203	4 414 607	4 954 368	5 523 101	$81(\frac{3}{2})[\frac{5}{2}]$	$15(\frac{3}{2})[\frac{3}{2}]$	$81(\frac{3}{2})[\frac{5}{2}]$	$18(\frac{3}{2})[\frac{3}{2}]$	^3D
$3p(\frac{3}{2})[\frac{3}{2}]$	2	2 993 584	3 445 090	3 926 887	4 438 597	4 982 062	5 555 050	$83(\frac{3}{2})[\frac{3}{2}]$	$17(\frac{3}{2})[\frac{5}{2}]$	$82(\frac{3}{2})[\frac{3}{2}]$	$18(\frac{3}{2})[\frac{5}{2}]$	^1D
	1	2 986 739	3 437 344	3 918 095	4 428 554	4 970 636	5 542 158	$90(\frac{3}{2})[\frac{3}{2}]$	$10(\frac{1}{2})[\frac{3}{2}]$	$94(\frac{3}{2})[\frac{3}{2}]$		^3D
$3p(\frac{3}{2})[\frac{1}{2}]$	1	2 953 558	3 401 413	3 879 444	4 387 211	4 926 429	5 494 974	$87(\frac{3}{2})[\frac{1}{2}]$	$13(\frac{1}{2})[\frac{1}{2}]$	$90(\frac{3}{2})[\frac{1}{2}]$	$6(\frac{1}{2})[\frac{1}{2}]$	^3S
	0	3 009 192	3 464 198	(3 949 776)	4 466 070	4 014 563	(5 592 735)	$55(\frac{1}{2})[\frac{1}{2}]$	$45(\frac{3}{2})[\frac{1}{2}]$	$55(\frac{3}{2})[\frac{1}{2}]$	$45(\frac{1}{2})[\frac{1}{2}]$	^3P
$3p(\frac{1}{2})[\frac{3}{2}]$	2	3 016 780	3 474 958	3 965 425	4 487 045	5 041 714	5 628 520	$96(\frac{1}{2})[\frac{3}{2}]$		$99(\frac{1}{2})[\frac{3}{2}]$		^3P
	1	3 007 333	3 463 292	3 951 159	4 469 715	5 020 941	5 603 789	$88(\frac{1}{2})[\frac{3}{2}]$	$10(\frac{3}{2})[\frac{3}{2}]$	$91(\frac{1}{2})[\frac{3}{2}]$	$6(\frac{1}{2})[\frac{1}{2}]$	^1P
$3p(\frac{1}{2})[\frac{1}{2}]$	1	3 017 220	3 474 958	3 964 847	4 485 944	5 039 971	5 626 306	$85(\frac{1}{2})[\frac{1}{2}]$	$13(\frac{3}{2})[\frac{1}{2}]$	$88(\frac{1}{2})[\frac{1}{2}]$	$7(\frac{1}{2})[\frac{3}{2}]$	^3P
	0	(3 100 856)	3 564 763	(4 060 537)	4 585 819	5 143 616	(5 732 942)	$55(\frac{3}{2})[\frac{1}{2}]$	$45(\frac{1}{2})[\frac{1}{2}]$	$55(\frac{1}{2})[\frac{1}{2}]$	$45(\frac{3}{2})[\frac{1}{2}]$	^1S
$3d(\frac{3}{2})[\frac{7}{2}]$	4	3 208 329	3 678 797	4 179 462	4 710 105	5 272 468	5 864 439	$100(\frac{3}{2})[\frac{7}{2}]$		$100(\frac{3}{2})[\frac{7}{2}]$		^3F
	3	3 212 375	3 683 330	4 184 514	4 715 469	5 278 128	5 870 337	$84(\frac{3}{2})[\frac{7}{2}]$	$11(\frac{3}{2})[\frac{5}{2}]$	$87(\frac{3}{2})[\frac{7}{2}]$	$11(\frac{3}{2})[\frac{5}{2}]$	^3F
$3d(\frac{3}{2})[\frac{5}{2}]$	3	3 224 367	3 696 911	4 199 685	4 732 377	5 296 812	5 890 952	$84(\frac{3}{2})[\frac{5}{2}]$	$13(\frac{3}{2})[\frac{7}{2}]$	$88(\frac{3}{2})[\frac{5}{2}]$	$12(\frac{3}{2})[\frac{7}{2}]$	^1F
	2	3 219 669	3 691 702	4 193 932	4 726 016	5 289 794	5 883 137	$89(\frac{3}{2})[\frac{5}{2}]$	$11(\frac{1}{2})[\frac{5}{2}]$	$97(\frac{3}{2})[\frac{5}{2}]$		^3F

TABLE V. (*Continued*).

Designation	J	Ca XI	Sc XII	Ti XIII	V XIV	Cr XV	Mn XVI	Eigenvector components (%)[a] Ca XI		Mn XVI		LS designation[b]
$3d(\frac{3}{2})[\frac{3}{2}]$	2	3 205 269	3 675 982	4 177 038	4 708 057	5 270 945	5 863 347	$85(\frac{3}{2})[\frac{3}{2}]$	$15(\frac{1}{2})[\frac{3}{2}]$	$93(\frac{3}{2})[\frac{3}{2}]$	$7(\frac{1}{2})[\frac{3}{2}]$	^3P
	1	3 239 700[e]	3 714 318	4 219 800[e]	4 757 800[e]	5 324 200[e]	5 923 500[e]	$60(\frac{3}{2})[\frac{3}{2}]$	$30(\frac{1}{2})[\frac{3}{2}]$	$63(\frac{3}{2})[\frac{3}{2}]$	$19(\frac{1}{2})[\frac{3}{2}]$	^3D
		(3 239 049)		(4 220 304)	(4 756 353)	(5 324 332)	(5 922 349)					
$3d(\frac{3}{2})[\frac{1}{2}]$	1	3 199 035	3 668 546	4 168 326	(4 697 819)	5 259 419	5 850 249	$69(\frac{3}{2})[\frac{1}{2}]$	$25(\frac{3}{2})[\frac{3}{2}]$	$68(\frac{3}{2})[\frac{1}{2}]$	$29(\frac{3}{2})[\frac{3}{2}]$	^3P
	0	(3 195 852)	(3 664 729)	4 163 874	(4 692 510)	5 253 448	5 843 409	$100(\frac{3}{2})[\frac{1}{2}]$		$100(\frac{3}{2})[\frac{1}{2}]$		^3P
$3d(\frac{1}{2})[\frac{5}{2}]$	3	3 248 488	3 727 574	4 238 843	4 781 291	5 356 770	5 964 431	$94(\frac{1}{2})[\frac{5}{2}]$		$98(\frac{1}{2})[\frac{5}{2}]$		^3D
	2	3 244 581	3 722 705	4 233 020	4 774 275	5 348 574	(5 955 038)	$89(\frac{1}{2})[\frac{5}{2}]$	$11(\frac{3}{2})[\frac{5}{2}]$	$96(\frac{1}{2})[\frac{5}{2}]$		^1D
$3d(\frac{1}{2})[\frac{3}{2}]$	2	(3 248 233)	3 726 769	4 237 394	4 779 239	5 354 045	5 961 148	$85(\frac{1}{2})[\frac{3}{2}]$	$15(\frac{3}{2})[\frac{3}{2}]$	$93(\frac{1}{2})[\frac{3}{2}]$	$7(\frac{3}{2})[\frac{3}{2}]$	^3D
	1	3 284 300[e]	3 767 300[e]	4 281 600[e]	4 827 200[e]	5 406 300[e]	6 018 300[e]	$64(\frac{1}{2})[\frac{3}{2}]$	$21(\frac{3}{2})[\frac{1}{2}]$	$78(\frac{1}{2})[\frac{3}{2}]$	$14(\frac{3}{2})[\frac{1}{2}]$	^1P
		(3 283 425)	(3 767 124)	(4 281 767)	(4 827 075)	(5 405 544)	(6 015 407)					

[a]Only the two largest components are given. Components smaller than 5% are omitted.
[b]LS designations used in previous work (Refs. 5—7), corresponding to the leading LS component in the beginning of the sequence.
[c]Levels determined from the resonance lines in the soft x-ray region. All the other level values are determined relative to these levels.
[d]Derived through isoelectronic interpolation (see text).
[e]Level value determined from transitions to the ground state, previously reported in the literature (Refs. 22—24). The level cannot be connected to the rest of the levels by transitions observed in the present work.

TABLE VI. Energy levels (cm^{-1}) of the $2p^54s$ and $4p$ configurations.

Designation	J	Ca XI	Sc XII	Ti XIII	V XIV	Cr XV	Mn XVI
$4s(\frac{3}{2},\frac{1}{2})$	2	3 752 565	4 337 350	4 963 878		6 340 270	7 089 864
	1	3 753 900[a]	4 339 300[a]	4 966 500[a]	5 632 000[a]	6 346 291	7 092 000[a]
$4s(\frac{1}{2},\frac{1}{2})$	1	3 781 900[a]	4 378 800[a]	5 014 300[a]	5 690 000[a]	6 412 678	
	0					6 410 346	
$4p(\frac{3}{2})[\frac{5}{2}]$	3	3 818 112	4 409 384	5 047 533	5 721 285	6 438 194	7 195 714
	2					6 435 277	
$4p(\frac{3}{2})[\frac{3}{2}]$	2					6 445 145	
	1					6 441 300	7 198 860
$4p(\frac{3}{2})[\frac{1}{2}]$	1					6 428 094	7 184 624
	0						
$4p(\frac{1}{2})[\frac{3}{2}]$	2	3 850 940	4 450 987		5 782 170	6 511 590	7 283 910
	1					6 503 510	
$4p(\frac{1}{2})[\frac{1}{2}]$	1						
	0						

[a]Level value determined from transition to the ground state (Ref. 24).

No lines have been found that connect levels having different parent states ($^2P_{1/2}$ and $^2P_{3/2}$). A direct connection would be given by the magnetic dipole transition within the $3s$ configuration, viz., from the metastable $(\frac{1}{2},\frac{1}{2})_0$ level to $(\frac{3}{2},\frac{1}{2})_1$, and in fact a line in a solar flare spectrum has been identified as this transition in Fe XVII.[4] Another line connecting the two parent systems has been reported in Ti XIII,[25] and it might be possible to use these observations for interpolating the $^2P_{1/2}$-$^2P_{3/2}$ interval.[26] Pending more accurate observations, e.g., of the magnetic dipole transition in tokamak plasmas, the relative positions of the two sets of levels are determined in the present work by the x-ray transitions to the ground state. Predicted wavelengths for the magnetic dipole transition derived from the energy levels of Table V are given in Table VIII. The table also contains predicted wavelengths for the magnetic quadrupole transition from the metastable $3s(\frac{3}{2},\frac{1}{2})_2$ level to the ground state. This transition has been observed in Cr XV in a tokamak plasma.[27]

V. TERM STRUCTURE

The structure of the $2p^5nl$ configurations in highly charged neonlike ions is dominated by the large spin-orbit interaction within the $2p^5$ core. The levels are thus split in two separate groups, correlated to the $^2P_{3/2}$ and $^2P_{1/2}$ states of the inverted parent term. Representations other than the *LS* scheme that give the most appropriate descriptions of the level structure will be discussed for each configuration below.

As Z increases, the $2s2p^63l$ configurations move downwards through the term system to positions close to $2s^22p^53l$. These two groups of configurations have the same set of principal quantum numbers, which gives large interaction integrals. This means that the resulting perturbations may be significant even at large distances between the interacting configurations,[11,28] but they vary smoothly along the isoelectronic sequence. Perturbations may also occur where the $2s2p^63l$ configurations cross the $2s^22p^54l$ configurations of the same parity, but in these cases the interaction integrals are small and the perturbations are large only at small distances between the interacting states. The possible positions for such local perturbations can be found in Fig. 5, where the configuration average energies predicted by Hartree-Fock wave functions are shown for Al IV—Fe XVII. The perturbations of $4d$ in Cl VIII and $4s$ in K X caused by $2s2p^63p$ were found and discussed already by Edlén and Tyrén.[22] Drastic perturbations of this kind have been observed in the present work and will be discussed in connection with the $n=4$ configurations.

The *ab initio* wave functions and Slater intervals were obtained from the Froese Fischer MCHF72 computer program[29] used in the single-configuration mode. These integrals were used as input to the matrix program of Cowan,[30] which calculates the angular matrices, diagonalizes them, and provides eigenvectors in various coupling schemes. The integral values were adjusted by a least-squares program of Cowan to fit the observed levels.

A. The $2p^53l$ configurations

The fitted energy parameters and the Hartree-Fock energy integrals for the $3s$, $3p$, and $3d$ configurations are shown in Tables IX—XI. The structure of the $n=3$ configurations has been analyzed previously in Ca XI (Ref. 6) and Ti XIII (Ref. 5), and the predicted isoelectronic trends of the scaling factors for the *ab initio* integrals are fully confirmed in the present work. In particular the ratios between the fitted and the *ab initio* values of the configuration average energies are seen to approach a minimum close to unity and then increase again. This behavior, caused by decreasing correlation and increasing relativistic effects as Z increases, is discussed in detail in Ref. 11. It

TABLE VII. Energy levels (cm^{-1}) of the $2p^54d$ and $4f$ configurations.

Designation	J	Ca XI	Sc XII	Ti XIII	V XIV	Cr XV	Mn XVI	Eigenvector components (%)[a] Ca XI		Mn XVI	
$4d(\frac{3}{2})[\frac{7}{2}]$	4	3 902 243	4 502 941	5 144 529	5 827 194	6 552 477	7 317 468	$100(\frac{3}{2})[\frac{7}{2}]$		$100(\frac{3}{2})[\frac{7}{2}]$	
	3	3 904 085	4 504 960	5 146 743	5 829 497	6 554 730	7 319 729	$88(\frac{3}{2})[\frac{7}{2}]$	$12(\frac{3}{2})[\frac{5}{2}]$	$88(\frac{3}{2})[\frac{7}{2}]$	$12(\frac{3}{2})[\frac{5}{2}]$
$4d(\frac{3}{2})[\frac{5}{2}]$	3	3 908 352	4 509 787	5 152 207	5 835 457	(6 561 316)	7 327 149	$88(\frac{3}{2})[\frac{5}{2}]$	$12(\frac{3}{2})[\frac{7}{2}]$	$88(\frac{3}{2})[\frac{5}{2}]$	$12(\frac{3}{2})[\frac{7}{2}]$
	2	3 096 966	4 508 125	5 150 335	5 833 302	6 559 009	7 324 359	$99(\frac{3}{2})[\frac{5}{2}]$		$99(\frac{3}{2})[\frac{5}{2}]$	
$4d(\frac{3}{2})[\frac{3}{2}]$	2	3 902 793	4 503 623	5 145 204	(5 828 206)	6 553 480	7 318 722	$97(\frac{3}{2})[\frac{3}{2}]$		$98(\frac{3}{2})[\frac{3}{2}]$	
	1	3 919 000[b]	4 521 000[b]	5 163 700[b]	5 850 000[b]	6 577 496	7 344 868	$65(\frac{3}{2})[\frac{3}{2}]$	$25(\frac{3}{2})[\frac{1}{2}]$	$63(\frac{3}{2})[\frac{3}{2}]$	$33(\frac{3}{2})[\frac{3}{2}]$
		(3 918 031)	(4 520 968)	(5 164 907)	(5 849 876)						
$4d(\frac{3}{2})[\frac{1}{2}]$	1	(3 899 838)	4 500 231	5 141 514	5 823 811	6 548 779	7 313 554	$67(\frac{3}{2})[\frac{1}{2}]$	$31(\frac{3}{2})[\frac{3}{2}]$	$64(\frac{3}{2})[\frac{1}{2}]$	$35(\frac{3}{2})[\frac{3}{2}]$
	0	(3 898 100)	(4 498 236)	(5 139 143)	5 821 381	6 545 969	7 310 174	$100(\frac{3}{2})[\frac{1}{2}]$		$100(\frac{3}{2})[\frac{1}{2}]$	
$4d(\frac{1}{2})[\frac{5}{2}]$	3	3 935 805	4 544 404	5 196 075	5 889 775	6 627 484	7 407 660	$99(\frac{1}{2})[\frac{5}{2}]$		$100(\frac{1}{2})[\frac{5}{2}]$	
	2	3 933 881	4 542 191	5 193 359	5 886 695	6 624 071	7 403 649	$98(\frac{1}{2})[\frac{5}{2}]$		$98(\frac{1}{2})[\frac{5}{2}]$	
$4d(\frac{1}{2})[\frac{3}{2}]$	2	3 934 786	4 543 198	5 194 527	5 888 124	6 625 741	7 405 446	$97(\frac{1}{2})[\frac{3}{2}]$		$97(\frac{1}{2})[\frac{3}{2}]$	
	1	3 948 400[b]	4 557 900[b]	5 207 200[b]	5 904 000[b]	6 641 000[b]	7 429 000[b]	$88(\frac{1}{2})[\frac{3}{2}]$	$8(\frac{3}{2})[\frac{1}{2}]$	$95(\frac{1}{2})[\frac{3}{2}]$	
		(3 948 274)	(4 557 776)	(5 210 021)	(5 904 531)	(6 643 082)	(7 423 789)				
$4f(\frac{3}{2})[\frac{9}{2}]$	5	3 936 559	4 542 083	5 188 812	5 876 175	6 606 248	7 376 639	$100(\frac{3}{2})[\frac{9}{2}]$		$100(\frac{3}{2})[\frac{9}{2}]$	
	4	3 936 645	4 542 110	5 188 814	5 876 259	6 606 203	7 376 520	$100(\frac{3}{2})[\frac{9}{2}]$		$100(\frac{3}{2})[\frac{9}{2}]$	
$4f(\frac{3}{2})[\frac{7}{2}]$	4	3 939 164	4 545 094	5 192 205	5 879 941	6 610 470	7 381 282	$100(\frac{3}{2})[\frac{7}{2}]$		$100(\frac{3}{2})[\frac{7}{2}]$	
	3	3 938 963	4 544 885	5 191 932	5 879 633	6 610 006	7 380 720	$100(\frac{3}{2})[\frac{7}{2}]$		$91(\frac{3}{2})[\frac{7}{2}]$	$9(\frac{3}{2})[\frac{5}{2}]$
$4f(\frac{3}{2})[\frac{5}{2}]$	3	3 944 822	4 546 279	5 192 368	5 879 567	6 609 778	7 380 185	$82(\frac{3}{2})[\frac{5}{2}]$	$14\,^3D$	$91(\frac{3}{2})[\frac{5}{2}]$	$9(\frac{3}{2})[\frac{7}{2}]$
	2	(3 945 882)	4 546 089	(5 192 357)	(5 879 576)	(6 609 750)	(7 380 285)	$67(\frac{3}{2})[\frac{5}{2}]$	$20\,^1D$	$94(\frac{3}{2})[\frac{5}{2}]$	$6(\frac{3}{2})[\frac{3}{2}]$
$4f(\frac{3}{2})[\frac{3}{2}]$	2	3 953 315	4 546 312	5 191 256	(5 877 958)	6 607 601	7 377 669	$51(\frac{3}{2})[\frac{3}{2}]$	$40\,^3D$	$94(\frac{3}{2})[\frac{3}{2}]$	$6(\frac{3}{2})[\frac{5}{2}]$
	1	(3 950 491)	(4 546 140	5 191 014	(5 877 442)	6 606 943	7 376 779	$69(\frac{3}{2})[\frac{3}{2}]$	$31\,^3D$	$99(\frac{3}{2})[\frac{3}{2}]$	
$4f(\frac{1}{2})[\frac{7}{2}]$	4	3 967 641	4 581 021	5 237 513	5 935 911	6 678 300	7 463 551	$100(\frac{1}{2})[\frac{7}{2}]$		$100(\frac{1}{2})[\frac{7}{2}]$	
	3	3 967 634	4 580 818	5 237 320	5 935 375	6 677 634	(7 462 863)	$100(\frac{1}{2})[\frac{7}{2}]$		$100(\frac{1}{2})[\frac{7}{2}]$	
$4f(\frac{1}{2})[\frac{5}{2}]$	3	(3 972 931)	4 583 224	5 239 054	5 937 239	6 679 495	7 464 838	$90(\frac{1}{2})[\frac{5}{2}]$	$10\,^3D$	$99(\frac{1}{2})[\frac{5}{2}]$	
	2	(3 973 119)	(4 583 089)	(5 238 860)	(5 937 160)	(6 679 422)	(7 464 658)	$87(\frac{1}{2})[\frac{5}{2}]$	$12\,^1D$	$100(\frac{1}{2})[\frac{5}{2}]$	

[a]Only the two largest components are given. Components smaller than 5% are omitted. For $4f$, the contribution to the eigenvector from $3s3p^63d$ is given in LS designation.
[b]Level value determined from transition to the ground state (Ref. 24). Predicted values from a parametric calculation are given in parentheses.

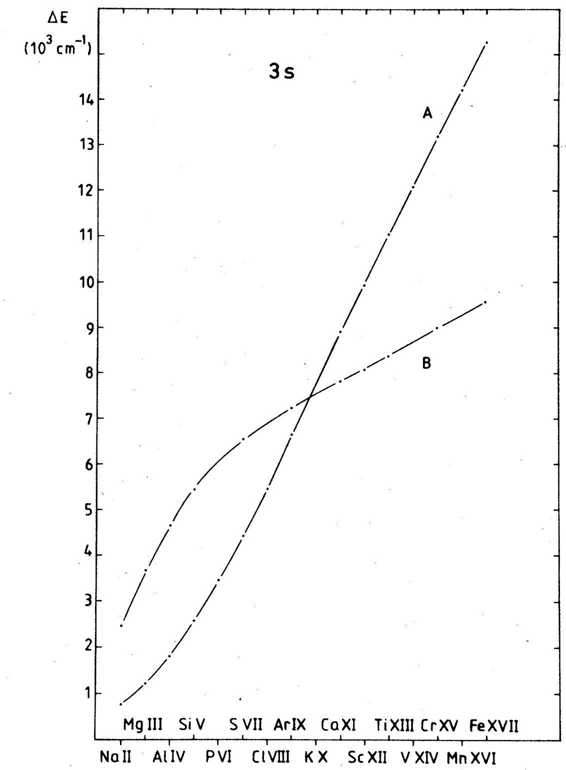

FIG. 4. Intervals in the $2p^53s$ configuration. Curve *A*: $(\frac{3}{2},\frac{1}{2})_1$-$(\frac{3}{2},\frac{1}{2})_2$. Curve *B*: $(\frac{1}{2},\frac{1}{2})_1$-$(\frac{1}{2},\frac{1}{2})_0$. The missing intervals in V XIV and Mn XVI have been determined through interpolation along a least-squares-fitted straight line from Ca XI to Fe XVII.

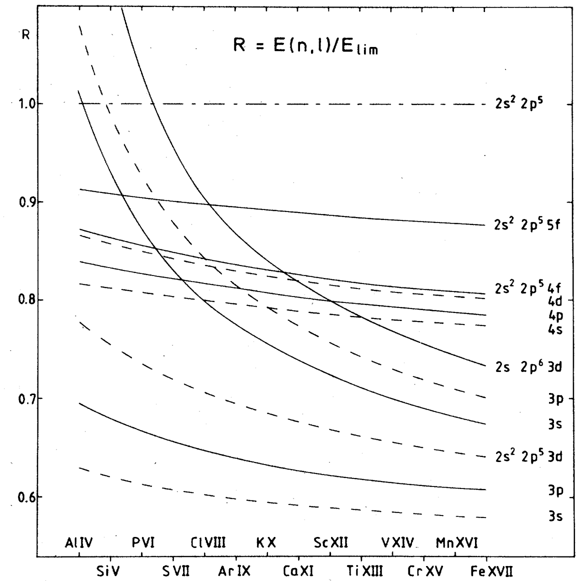

FIG. 5. Survey diagram of some excited configurations in the neonlike isoelectronic sequence. The average energy of each configuration, calculated from Hartree-Fock wave functions, is plotted as a function of the nuclear charge. The energy is scaled by the distance between the $2s^22p^6$ ground state and the ionization limit $2s^22p^5$. Even and odd configurations are represented by solid and dashed curves, respectively. It is seen that strong local perturbations due to interaction between $2s^22p^54l$ and $2s2p^63l$ may occur in the ions S VII—Sc XII.

should be noted that the parameters for Ti XIII have been changed somewhat from Ref. 5 due to the addition of levels derived from beam-foil data.

As can be seen in Table V, the $3s$ levels are given *jj* designations. The eigenvector components, shown in the table for Ca XI and Mn XVII, reveal that the purity in *jj* coupling is high, and that it increases with increasing Z as expected. The average purity for $3s$ in *jj* coupling is 98% in Mn XVI. The *LS* designations shown at the right-hand part of the table correspond to the appropriate level designations in the beginning of the sequence, but they are not

TABLE VIII. Predicted wavelengths (Å) in vacuum for magnetic dipole and quadrupole transitions from $3s$ levels.

Ion	Predicted wavelengths (Å) $3s(\frac{3}{2},\frac{1}{2})_1$-$(\frac{1}{2},\frac{1}{2})_0$	$2p^6\,{}^1S_0$-$3s(\frac{3}{2},\frac{1}{2})_2$
Ca XI	4718.1	35.688
Sc XII	3619.3	30.910
Ti XIII	2774.8	27.041
V XIV	2187.7	23.863
Cr XV	1764.5	21.212[a]
Mn XVI	1422.1	18.986

[a]Observed wavelength 21.213 Å (Ref. 27).

applicable to the ions discussed here (except for $J=0$ and 2, which are pure in both schemes).

As in $3s$, *LS* designations do not describe the $3p$ and $3d$ levels properly. Here the coupling is, however, still intermediate, and no representation gives eigenvectors of high purity for all the levels. It could be discussed whether the er the ultimate coupling asymptotically approached at high Z will be *jj* or *jl*,[31] and, in fact, *jj* designations have been used in the relativistic calculations by Cogordan and Lunell.[13] We have, however, chosen *jl* designations in the present work for different reasons: (i) the average purity is higher in *jl* than in *jj* representation for the ions treated here, (ii) *jl* notation is generally used in the compilations of previous work,[24] and (iii) the $4d$ and $4f$ configurations show high purity in the *jl* representation, and the $3p$-$4d$ and $3d$-$4f$ transition arrays have the pronounced diagonal character typical for *jl* coupling (strongest lines where $\Delta J=\Delta K$). The *jl* eigenvector components are shown in Table V, and in most cases the purity is seen to be high. The average purities in *jl* coupling in Mn XVI are 82 and 86% for $3p$ and $3d$. For convenience the *LS* designations corresponding to the maximum eigenvector components in the beginning of the sequence and used in Refs. 5—7 are shown in Table IV. In several cases these designations do not agree with the low purity maximum *LS* components for the ions treated here. It should be noted that even in *jl* representation, the purity of the $3p$ $J=0$ levels is low, and that the designations in Ca XI are chosen ac-

TABLE IX. Energy parameters (cm^{-1}) for $2s^22p^53s$. The first row for each parameter gives the fitted value. The second row contains the Hartree-Fock value for the corresponding energy integral, while the ratio between these two quantities is given in the third row. N is the number of fitted levels; σ is the rms deviation of the calculated levels.

	Ca XI	Sc XII	Ti XIII	V XIV	Cr XV	Mn XVI
$E_{av}(3s)$	2 816 246	3 252 201	3 718 712	4 215 080	4 743 161	5 301 050
	2 813 070	3 249 693	3 716 783	4 214 377	4 742 473	5 301 053
	1.0011	1.0008	1.0005	1.0002	1.0001	1.0000
$G^1(ps)$	24 914	26 965	29 049	31 171	33 353	35 297
	25 639	27 809	29 968	32 117	34 259	36 393
	0.97	0.97	0.97	0.97	0.97	0.97
$\zeta(2p)$	19 991	24 997	31 342	38 496	46 523	56 285
	19 615	24 721	30 763	37 848	46 090	55 608
	1.02	1.01	1.02	1.02	1.01	1.01
N	4	4	4	4	4	4
σ	33	69	77	62	99	131

cording to the isoelectronic trend and do not correspond to the maximum eigenvector components.

The level designations used here are an abbreviated form of the jK notation. Thus $2p^5(^2P_{J1})nl[K]_J$ is written $nl(J1)[K]_J$. In the figures the parent state is further abbreviated, so that $[K]$ stands for $(\frac{3}{2})[K]$ and $[K]'$ for $(\frac{1}{2})[K]$.

As mentioned previously, both $3p$ and $3d$ are affected by long-range perturbations from $2s2p^63l$. Due to the lack of information on these configurations and the slowly changing magnitude of the perturbations along the sequence, it has not been possible to treat the interaction in detail. The perturbations are instead taken care of by the effective parameter D^1 in the fitting procedure. The introduction of this parameter significantly reduces the standard deviation of the fitted levels shown in the last row of Tables X and XI, but the derived values of the parameter are uncertain and show a somewhat irregular behavior. A more exact treatment will be possible when accurate data on $2s2p^63l$ become available.

Due to the difficulty mentioned above to establish two of the $J=1$ levels of $3d$, it was necessary to fix the value of $G^1(2p,3d)$ at a scaled Hartree-Fock value in the parametric fit. The scaling factor was obtained through

TABLE X. Energy parameters (cm^{-1}) for $2s^22p^53p$. The first row for each parameter gives the fitted value. The second row contains the Hartree-Fock value for the corresponding energy integral, while the ratio between these two quantities is given in the third row. Parentheses mean that the parameter was fixed during the fitting procedure. N is the number of fitted levels; σ is the rms deviation of the calculated levels.

	Ca XI	Sc XII	Ti XIII	V XIV	Cr XV	Mn XVI
$E_{av}(3p)$	2 994 352	3 447 118	3 930 707	4 444 491	4 990 316	5 566 390
	2 985 676	3 437 564	3 919 874	4 432 660	4 975 924	5 549 652
	1.0029	1.0028	1.0028	1.0027	1.0029	1.0030
$F^2(pp)$	73 772	80 631	86 937	93 682	100 655	106 616
	63 742	69 636	75 504	81 353	87 184	93 000
	1.16	1.16	1.15	1.15	1.15	1.15
$G^0(pp)$	(23 650)	25 972	(28 415)	30 700	33 034	(35 450)
	25 293	27 609	29 910	32 196	34 471	36 736
	(0.94)	0.94	(0.95)	0.95	0.96	(0.96)
$G^2(pp)$	27 617	30 198	33 179	35 654	38 349	40 852
	27 052	29 655	32 246	34 826	37 397	39 961
	1.02	1.02	1.03	1.02	1.03	1.02
$\zeta(2p)$	19 863	24 846	31 204	38 358	46 353	56 165
	19 628	24 735	30 778	37 863	46 104	55 621
	1.01	1.00	1.01	1.01	1.01	1.01
$\zeta(3p)$	3982	5150	6591	8345	10 307	12 749
	3548	4645	5972	7559	9435	11 635
	1.12	1.11	1.10	1.10	1.09	1.10
D^1	4503	4660	5231	5364	5409	5851
N	9	10	8	10	10	8
σ	74	150	42	103	228	119

TABLE XI. Energy parameters (cm^{-1}) for $2s^22p^53d$. The first row for each parameter gives the fitted value. The second row contains the Hartree-Fock value for the corresponding energy integral, while the ratio between these two quantities is given in the third row. Parentheses mean that the parameter was fixed during the fitting procedure. N is the number of fitted levels; σ is the rms deviation of the calculated levels.

	Ca XI	Sc XII	Ti XIII	V XIV	Cr XV	Mn XVI
$E_{av}(3d)$	3 227 013	3 701 073	4 205 976	4 741 152	5 308 542	5 906 350
	3 215 888	3 688 065	4 190 881	4 723 880	5 287 308	5 881 036
	1.0035	1.0035	1.0037	1.0037	1.0040	1.0043
$F^2(pd)$	75 645	84 169	92 815	101 877	110 012	119 358
	74 430	82 966	91 471	99 947	108 396	116 821
	1.02	1.01	1.01	1.02	1.01	1.02
$G^1(pd)$	(54 470)	(62 429)	(69 780)	(77 136)	(84 494)	(91 850)
	62 605	70 942	79 295	87 655	96 016	104 375
	(0.87)	(0.88)	(0.88)	(0.88)	(0.88)	(0.88)
$G^3(pd)$	33 012	37 871	42 826	47 244	52 222	56 783
	35 869	40 694	45 533	50 380	55 230	60 082
	0.92	0.93	0.94	0.94	0.95	0.95
$\zeta(2p)$	19 976	24 997	31 374	38 545	46 580	56 378
	19 654	24 764	30 809	37 897	46 141	55 661
	1.02	1.01	1.02	1.02	1.01	1.01
$\zeta(3d)$	271	386	495	721	907	1164
	349	484	652	860	1113	1416
	0.78	0.80	0.76	0.84	0.81	0.82
D^1	2643	2896	2980	3332	2940	3065
N	8	10	10	8	10	9
σ	43	48	60	60	97	101

TABLE XII. Energy parameters (cm^{-1}) for $2s^22p^54d$. The first row for each parameter gives the fitted value. The second row contains the Hartree-Fock value for the corresponding energy integral, while the ratio between these two quantities is given in the third row. Parentheses mean that the parameter was fixed during the fitting procedure. N is the number of fitted levels; σ is the rms deviation of the calculated levels.

	Ca XI	Sc XII	Ti XIII	V XIV	Cr XV	Mn XVI
$E_{av}(4d)$	3 915 775	4 519 354	5 164 522	5 851 093	6 580 708	7 350 940
	3 900 599	4 502 282	5 145 161	5 829 231	6 554 534	7 320 935
	1.0039	1.0038	1.0038	1.0037	1.0040	1.0041
$F^2(pd)$	26 563	29 572	33 138	35 361	38 360	41 525
	26 773	29 683	32 587	35 487	38 382	41 275
	0.99	1.00	1.02	1.00	1.00	1.01
$G^1(pd)$	(23 041)	(25 724)	(28 390)	(31 043)	33 791	36 581
	24 001	26 796	29 573	32 336	35 085	37 823
	(0.96)	(0.96)	(0.96)	(0.96)	0.96	0.97
$G^3(pd)$	13 323	15 094	17 527	18 678	19 552	21 641
	14 120	15 804	17 482	19 155	20 822	22 484
	0.94	0.96	1.00	0.97	0.94	0.96
$\zeta(2p)$	20 107	25 133	31 526	38 698	46 836	56 695
	19 711	24 837	30 900	38 010	46 278	55 825
	1.02	1.01	1.02	1.02	1.01	1.02
$\zeta(4d)$	134	183	230	331	413	558
	136	187	252	331	428	543
	0.99	0.98	0.91	1.00	0.96	1.03
N	8	9	9	9	10	11
σ	17	33	81	72	86	132

isoelectronic extrapolation.[5] In the same way, $G^0(2p,3p)$ had to be fixed for $3p$ in Ca XI, Ti XIII, and Mn XVI. Level values derived from the fitted and extrapolated parameters are given in parentheses in Table V for levels that could not be established experimentally.

B. 4d

The energy levels of the $2p^54l$ configurations are shown in Tables VI and VII, and the energy integrals of $4d$ and $4f$ in Tables XII and XIII. The discussion will start with $4d$ as it is the most completely known $n=4$ configuration, essentially unaffected by perturbations.

The regular behavior of the $3p$-$4d$ transitions and the $4d$-level structure can be seen in Figs. 1 and 6. The figures also reveal the slight perturbations of certain levels in Cl VIII and Ar IX, caused by $2s2p^63p$ as expected from Fig. 5. No perturbations are, however, evident in Ca XI—Mn XVI, and no interaction or effective parameters had to be introduced in the parametric fit. The derived parameters and the *ab initio* integrals are shown in Table XII. The level purities are seen in Table VII to be generally high in jl coupling, the only significant exception being the mixing of the $J=1$ levels of the $J=\frac{3}{2}$ parent. However, Fig. 6 shows that the pair structure is not particularly prominent. The average jl purity in Mn XVI is 89%.

As for $3d$, two of the $4d$ $J=1$ levels decay most readily to the ground state, and they are therefore difficult to establish relative to the rest of the configuration. For this reason, $G^1(pd)$ was fixed during the parametric fit at a scaled Hartree-Fock value in Ca XI to V XIV, with the scaling factor derived through isoelectronic interpolation.

C. 4f

The $3d$-$4f$ transitions form an easily recognizable group of lines, but the positions of certain lines are severly affected by perturbations as shown in Fig. 2. Perturbations of the $4f$ structure had been noticed at lower ionization stages as large deviations of the fitted G^2 and G^4 parameters from Hartree-Fock values.[32–34] Preliminary calculations showed that the small perturbations in these ions could be absorbed by effective parameters, but in the present work the actual perturber, $2s2p^63d$, has been included in the calculations.

TABLE XIII. Energy parameters (cm^{-1}) for $2s^22p^54f+2s2p^63d$. The first row for each parameter gives the fitted value. The second row contains the corresponding energy integral calculated from Hartree-Fock wave functions. The value in the third row is the ratio between the fitted parameter and the HF integral. Values fixed in the fit are given in parentheses. N is the number of fitted levels; σ is the rms deviation of the calculated levels.

	Ca XI	Sc XII	Ti XIII	V XIV	Cr XV	Mn XVI
$E_{av}(4f)$	3 947 538	4 555 735	5 205 800	5 896 900	6 631 126	7 406 555
	3 931 473	4 537 715	5 185 217	5 873 961	6 603 981	7 375 122
	1.0041	1.0040	1.0040	1.0039	1.0041	1.0043
$F^2(pf)$	13 052	15 354	16 968	18 658	20 864	23 121
	12 777	14 611	16 483	18 389	20 323	22 281
	1.02	1.05	1.03	1.02	1.03	1.04
$G^2(pf)$	(1604)	(1945)	(2306)	(2685)	(3081)	(3490)
	1887	2288	2713	3159	3625	4106
	(0.85)	(0.85)	(0.85)	(0.85)	(0.85)	(0.85)
$G^4(pf)$	(977)	(1185)	(1406)	(1638)	(1879)	(2130)
	1221	1481	1580	2047	2349	2662
	(0.80)	(0.80)	(0.80)	(0.80)	(0.80)	(0.80)
$\zeta(2p)$	20 082	25 160	31 575	38 775	46 885	56 753
	19 746	24 880	30 954	38 074	46 355	55 916
	1.02	1.01	1.02	1.02	1.01	1.02
$\zeta(4f)$	(36)	(52)	(70)	(95)	(125)	(162)
	33	47	64	86	114	147
	(1.1)	(1.1)	(1.1)	(1.1)	(1.1)	(1.1)
$E_{av}(3d)$	3 922 175	4 438 645	4 998 203	5 596 319	6 245 182	6 927 936
	3 905 035	4 422 655	4 970 600	5 548 934	6 157 716	6 796 792
	1.0044	1.0036	1.0056	1.0085	1.0142	1.0193
$G^2(sd)$	(56 469)	(64 470)	(72 519)	(80 599)	(88 699)	(96 811)
	56 469	64 470	72 519	80 599	88 699	96 811
$\zeta(3d)$	(314)	(438)	(594)	(788)	(1024)	(1308)
	314	438	594	788	1024	1308
$R^1(sf,pd)$	(−51 055)	(−56 980)	(−62 939)	(−68 925)	(−74 932)	(−80 955)
	−51 055	−56 980	−62 939	−68 925	−74 932	−80 955
$R^2(sf,pd)$	(−9732)	(−11 470)	(−13 268)	(−15 114)	(−17 003)	(−18 926)
	−9732	−11 470	−13 268	−15 114	−17 003	−18 926
N	8	10	10	8	10	9
σ	78	36	78	68	35	58

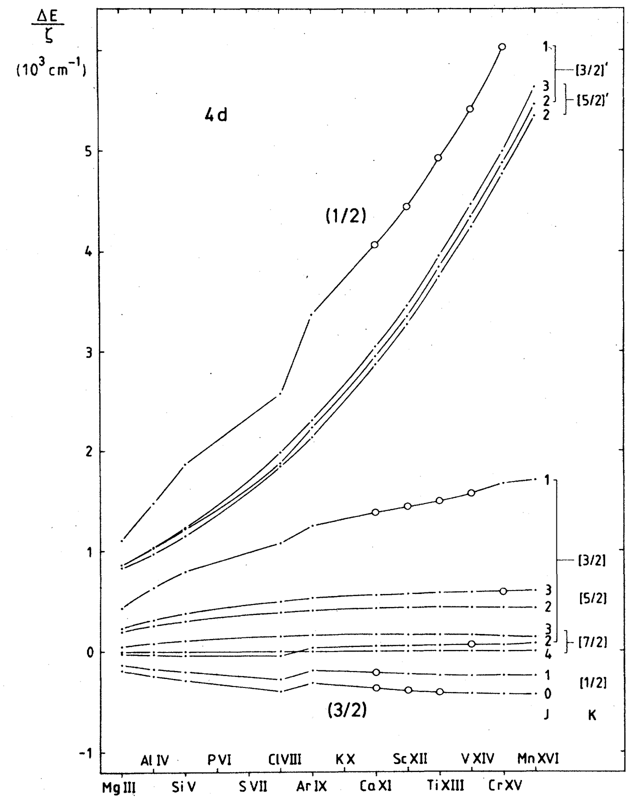

FIG. 6. Energy level structure of $2s^2 2p^5 4d$. The circles represent level values derived from fitted energy parameters in Ca XI—Mn XVI in cases where it was not possible to establish the levels from the present observations. A number of the levels are seen to be depressed in Cl VIII and pushed up in Ar IX due to interaction with $2s2p^6 3p$.

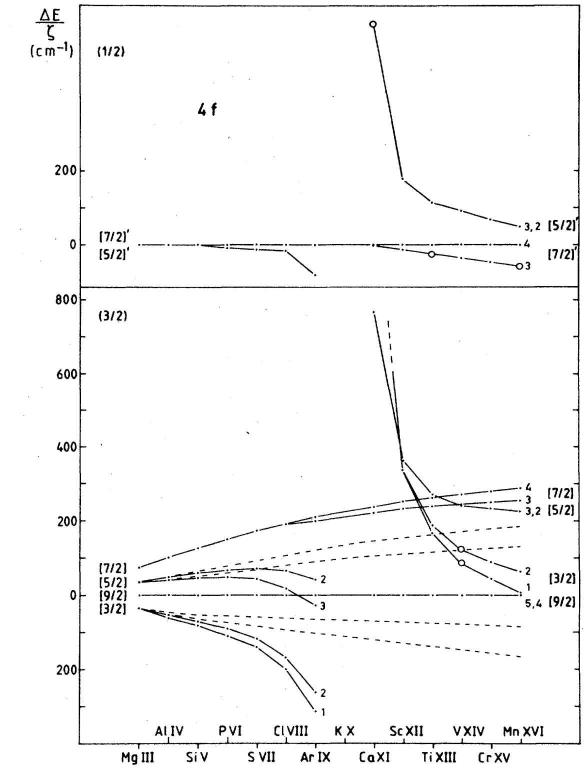

FIG. 7. Level structure of $2s^2 2p^5 4f$. As in Fig. 6, the circles represent predicted values for levels that could not be derived from the observed lines. As expected from the curves in Fig. 5, the structure is perturbed by $2s2p^6 3d$, which crosses $4f$ near K X. The dashed curves for the $(\frac{3}{2})[\frac{3}{2}]$ and $(\frac{3}{2})[\frac{5}{2}]$ levels represent Hartree-Fock predictions without configuration mixing.

The $4f$-level structure is shown in Fig. 7, where the two groups of levels based on the parent states with $J=\frac{1}{2}$ and $J=\frac{3}{2}$ are shown separately. In each case the positions are relative to the level with maximum J, which is unperturbed. The jl pair structure is evident, with the $(\frac{3}{2})[\frac{9}{2}]$ pair unresolved in the scale of the figure. For the $(\frac{1}{2})[\frac{5}{2}]$ and $(\frac{3}{2})[\frac{5}{2}]$ pairs only the predicted centers of gravity are shown, as the $J=2$ levels of these pairs could not be established. This is caused by the difficulty to establish the $J=1$ levels of $3d$.

The energy parameters and the *ab initio* integrals for $4f$ and $2s2p^6 3d$ are shown in Table XIII. The latter configuration has not been observed, and therefore its internal parameters and the interaction parameters were fixed at the Hartree-Fock values during the fit. The magnitude of the perturbation was allowed to vary by changing the average energy of the perturbing configuration. The small pair intervals and the fact that certain levels were missing for most or all of the ions made it difficult to obtain significant values for the small G^2, G^4, and ζ_{4f} parameters. For this reason they were fixed at scaled Hartree-Fock values, the scaling factors being chosen at the commonly found values of 0.8 for G^k and 1.0 for ζ. Thus the fits were made with only four free parameters.

The jl eigenvector components are shown in Table VII for Ca XI and Mn XVI. It is seen that the level purities are very high in Mn XVI, but the mixing with the $2s2p^6 3d$ levels, given in LS notation, is evident in Ca XI. It is significant also in Sc XII. The large perturbation in Ca XI made both the *ab initio* predictions and the isoelectronic extrapolations uncertain, and it was only possible to establish eight of the 12 $4f$ levels. The average jl purity in Mn XVI is 92%.

As can be seen in Fig. 7, the perturbation brings the $(\frac{3}{2})[\frac{7}{2}]_3$ and $(\frac{3}{2})[\frac{5}{2}]_3$ levels very close together in V XIV. This causes a strong mixing of the states, making the designation based on the eigenvector composition arbitrary. However, the combinations with $3d$ unambiguously point at the designations shown in Table VII.

For strict jl coupling[30] the higher energy level of a pair is that having even J when l_1+l_2 is even. A necessary condition is, however, that the pair splitting is mainly caused by the exchange interaction, and not by the spin-orbit interaction of the outer electron. The rule is not obeyed by the $4f(\frac{3}{2})[\frac{9}{2}]$ pair in the ions analyzed in this work, where the levels have the expected order in Ca XI and Sc XII, but the interval decreases to zero in Ti XIII and then increases again with the opposite order. The trend seems to be broken in V XIV, but this is caused by a blended line establishing the $J=4$ level. The explanation to the changed order can be found in the approximate formulas for the pair splittings in p^5f given by Humphreys *et al.*[35] Here it is seen that the interval of one pair, viz., $(\frac{3}{2})[\frac{9}{2}]$, is given by the difference of two terms in G^4 and ζ_{4f}. As the spin-orbit integral increases more rapidly than the exchange interaction along the sequence, the difference changes sign and the order of these two levels is reversed, just as observed here.

D. 4s

The $3p$-$4s$ lines are quite weak in the observed spectra, and it was possible to establish all the $4s$ levels only in Cr XV. No $3p$-$4s$ were found in V XIV, and in Ca, Sc, Ti, and Mn only transitions from the $J=2$ level of $4s$ could be identified with reasonable certainty. A reason for this is the fact that the $J=1$ levels as in $3d$ and $4d$ are mainly depopulated through transitions to the ground state. The $J=1$ level values derived from these transitions in the soft x-ray regions are shown in Table VI together with the levels derived in the present work.

No general parametric calculations have been made due to the small number of levels. A comparison between the observations and *ab initio* predictions show an improved agreement for the lower charge states when the interaction with $2s2p^63p$ is included in the calculations.

E. 4p

The $3s$-$4p$ lines are also weak, and it is difficult to identify more than a few lines unambiguously. Here the situation is complicated by the perturbation from $2s2p^63d$, which passes through $4p$ close to Sc XII. The perturbation effects the structure more severely in $4p$ than in $4f$, as all J values of $4p$ except $J=0$ occur in the perturbater. In fact also the $J=0$ levels may be perturbed, viz., by $2s2p^63s$.

Predictions with scaled Hartree-Fock parameters including the perturbation made it possible to identify a number of lines in Cr XV, and the stronger of them were found also in Mn XVI. The predictions and the observed intensities indicate that the lines $(\frac{3}{2},\frac{1}{2})_1$-$(\frac{3}{2})[\frac{3}{2}]_1$ and $(\frac{3}{2})(\frac{1}{2})_2$-$(\frac{3}{2})[\frac{1}{2}]_1$ coincide in these ions. In the lower charge states it has only been possible to identify the two strongest lines of the array except in Ti XIII, where only one line was found. No significant parametric calculations could of course be made at the small number of established levels. The isoelectronic trend of the two strongest lines is shown in Fig. 8.

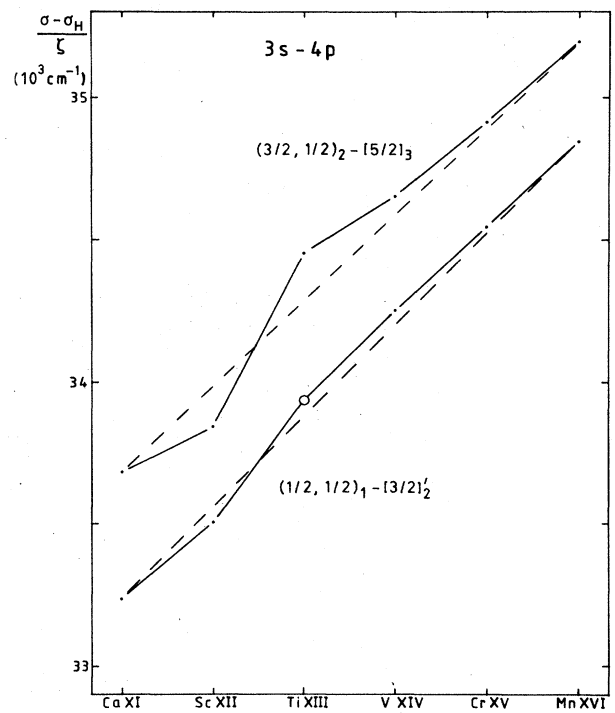

FIG. 8. The two strongest lines of the $3s$-$4p$ transition array. The quantity plotted is $(\sigma-\sigma_H)/\zeta$, where $\sigma_H=R\zeta^2(\frac{1}{9}-\frac{1}{16})$. In Ti XIII a predicted value from an *ab initio* calculation of the $4p$ structure is given for one of the lines, which was not observed. Dashed straight lines are drawn between Ca XI and Mn XVI to make visible the perturbation from $2s2p^63d$, which crosses $4p$ between Sc XII and Ti XIII.

VI. CONCLUSIONS

The present work greatly extends the knowledge of the $n=3$ and 4 configurations in the neonlike isoelectronic sequence. In particular it has demonstrated the influence from configuration crossings. The $n=3$ levels and the 3-3 transitions can be safely extrapolated to high values of Z, most accurately by using differences between the observations and relativistic calculations.[11,13] Concerning the $n=4$ levels and the 3-4 transitions, all the possible local perturbations caused by the crossings with $2s2p^63l$ appear before Ti XIII, and the structure at higher Z can be predicted, e.g., by extrapolating the scaling factors for the Hartree-Fock integrals. Even for $4s$ and $4p$, where it has been impossible to make complete analyses in most of the ions, the data for Cr XV form a good basis for further work.

ACKNOWLEDGMENTS

This work has been supported by the Swedish Natural Science Research Council (NFR) and the Swedish Energy Research Committee (Efn). In the United States it was supported in part by the U.S. Department of Energy, Office of Magnetic Fusion Energy.

[1]M. D. Rosen *et al.*, Phys. Rev. Lett. **54**, 106 (1985).
[2]D. L. Matthews *et al.*, Phys. Rev. Lett. **54**, 110 (1985).
[3]C. Jupén, Mon. Not. R. Astron. Soc. **208**, 1P (1984).
[4]U. Feldman, G. A. Doschek, and J. F. Seely, Mon. Not. R. Astron. Soc. **212**, 41P (1985).
[5]C. Jupén and U. Litzén, Phys. Scr. **30**, 112 (1984).
[6]C. Jupén, U. Litzén, and B. Skogvall, Phys. Scr. **33**, 69 (1986).
[7]C. Jupén and U. Litzén, Phys. Scr. **33**, 509 (1986).
[8]E. Träbert, Z. Phys. A **319**, 25 (1984).
[9]J. P. Buchet *et al.*, Phys. Scr. **31**, 364 (1985).
[10]M.-C. Buchet-Poulizac, J. P. Buchet, and S. Martin, J. Phys. (Paris) **47**, 407 (1986).
[11]J. A. Cogordan, S. Lunell, C. Jupén, and U. Litzén, Phys. Scr. **31**, 545 (1985).
[12]J. A. Cogordan, S. Lunell, C. Jupén, and U. Litzén, Phys. Rev. A **32**, 1885 (1985).
[13]J. A. Cogordan and S. Lunell, Phys. Scr. **33**, 406 (1986).
[14]E. P. Ivanova, L. N. Ivanov, A. E. Kramida, and A. V. Glushkov, Phys. Scr. **32**, 513 (1985).
[15]B. C. Fawcett, G. E. Bromage, and R. W. Hayes, Mon. Not. Roy. Astron. Soc. **186**, 113 (1979).
[16]S. O. Kastner, W. E. Behring, and L. Cohen, Astrophys. J. **199**, 777 (1975).
[17]J. Reader and N. Aquista, J. Opt. Soc. Am. **69**, 1285 (1979).
[18]J. Reader, G. Luther, and N. Aquista, J. Opt. Soc. Am. **69**, 144 (1979).
[19]J.-F. Wyart, J. Reader, and A. Ryabtsev, J. Opt. Soc. Am. **71**, 692 (1981).
[20]J. Reader and A. Ryabtsev, J. Opt. Soc. Am. **71**, 231 (1981).
[21]A. Ryabtsev and J. Reader, J. Opt. Soc. Am. **72**, 710 (1982).
[22]B. Edlén and F. Tyrén, Z. Phys. **101**, 206 (1936).
[23]F. Tyrén, Z. Phys. **111**, 314 (1938).
[24]C. Corliss and J. Sugar, Phys. Chem. Ref. Data **14**, Suppl. 2 (1985).
[25]E. Träbert, Z. Phys. D **1**, 283 (1986).
[26]C. Jupén and E. Träbert (unpublished).
[27]M. Klapisch *et al.*, Phys. Lett. **69A**, 34 (1978).
[28]J. E. Hansen, J. Phys. B **6**, 1751 (1973).
[29]C. Froese Fischer, Comput. Phys. Commun. **4**, 107 (1972).
[30]R. D. Cowan, *The Theory of Atomic Structure and Spectra* (University of California Press, Berkeley, 1981).
[31]The coupling, which can be formally written $[((l_1s_1)j_1,l_2)K,s_2]J$, is in the literature alternatively referred to as jl and jK. See, e.g., R. D. Cowan and K. L. Andrew, J. Opt. Soc. Am. **55**, 502 (1965).
[32]M.-C. Artru and V. Kaufman, J. Opt. Soc. Am. **65**, 594 (1975).
[33]L. W-Ü Brillet and M.-C. Artru, Phys. Scr. **14**, 285 (1976).
[34]C. Jupén, U. Litzén, and A. Trigueiros, Phys. Scr. **29**, 317 (1984).
[35]C. J. Humphreys, E. Paul, Jr., R. D. Cowan, and K. L. Andrew, J. Opt. Soc. Am. **57**, 855 (1967).